Acta Crystallographica Section B
Structural Science
ISSN 0108-7681

The structure of trititanate nanotubes

Q. Chen,[a] G.H. Du,[b] S. Zhang[a] and L.-M. Peng[a,b]*

[a]Department of Electronics, Peking University, Beijing 100871, People's Republic of China, and [b]Beijing Laboratory of Electron Microscopy, Chinese Academy of Sciences, PO Box 2724, Beijing 100080, People's Republic of China

Correspondence e-mail: plm@ele.pku.edu.cn

Received 19 September 2001
Accepted 20 May 2002

A comprehensive chemical and structural analysis is made of a new type of trititanate nanotube, which is synthesized *via* the reaction of TiO_2 particles with NaOH aqueous solution. It is found that the trititanate nanotubes are multi-walled scroll nanotubes with an inter-shell spacing of about 0.78 nm and an average diameter of about 9 nm. An atomic model of the nanotube is derived based on information from powder X-ray diffraction, selective-area electron diffraction, high-resolution electron microscopy and structure simulations. A model nanotube may be constructed by wrapping a (100) sheet of $H_2Ti_3O_7$ along [001] with the tube axis parallel to [010].

1. Introduction

Since the discovery of carbon nanotubes in 1991 by Iijima (Iijima, 1991), much research has been conducted on developing nanoscale tubular materials with novel properties, especially properties that are relevant to nanoelectronics. Besides carbon nanotubes, successful syntheses of nanotubes have been made of BN (Chopra *et al.*, 1995), $B_xC_yN_z$ (Weng-Sieh *et al.*, 1995), WS_2 (Tenne *et al.*, 1992), MoS_2 (Feldman *et al.*, 1995), $W_xMo_yC_zS_2$ (Hsu *et al.*, 2000), VO_x (Niederberger *et al.*, 2000) and TiO_2 (Kasuga *et al.*, 1998, 1999). Among these materials, the TiO_2 crystal has drawn particular attention owing to its excellent photocatalytic properties (Fukishima & Honda, 1972) and other potential applications in environmental purification, decomposition of carbonic acid gas and generation of hydrogen gas (Dagan & Tomkiewicz, 1993; Fukushima & Yamada, 1989). The tubular form of titanium oxide is especially important, since it has a larger surface area and higher photocatalytic activity (Adachi *et al.*, 2000). In an earlier work (Du *et al.*, 2001), we reported a successful synthesis of well crystallized nanoscale tubular materials *via* the reaction of TiO_2 particles and NaOH aqueous solution. It was found that neither the composition nor the structure of the synthesized nanotubes agree with that expected from tubes made of TiO_2 crystals with either anatase or rutile phases. Powder X-ray diffraction (XRD) shows very broad peaks that cannot be used to determine the structure of the nanotubes using normal XRD analysis methods.

In this paper, we will present a comprehensive structural investigation of our titanium oxide nanotubes using mainly advanced electron microscopy techniques and structure simulations. Our results show that the nanotubes are constructed from layered trititanate $H_2Ti_3O_7$.

2. Experimental

The nanoscale tubular materials used in this work were synthesized *via* the reaction of TiO_2 particles and NaOH

aqueous solution (Du *et al.*, 2001). Powder X-ray diffraction was performed with Cu $K\alpha$ radiation on a Rigaku D/max-2400 instrument. The transmission electron microscopy (TEM) sample was prepared by dispersing the materials in ethanol using ultrasonic treatment, dropping onto a holey carbon film supported on a copper grid and drying in air. A field-emission gun (FEG) TEM (Philips CM200/FEG with super-twin lens) equipped with a Gatan Imaging Filter (GIF) system was used for electron diffraction, TEM, high-resolution transmission electron microscopy (HRTEM) and electron energy-loss spectroscopy (EELS) work. Image simulations were carried out using the MSI software *CERIUS*^{2} (Accelrys, 2002) and a silicon graphics O2 computer workstation. IR spectra were obtained on a Nicolet Magna-IR 750 with a Nic Plan IR microscope.

3. Results and discussion

3.1. The tubular character

Fig. 1(*a*) is a typical experimental powder XRD profile taken from the sample. The figure shows that the diffraction peaks are much broader than those obtained from normal crystals, and thorough literature research shows that the profile cannot be attributed to any of the known crystal structures. Structure determination based on this profile only is not possible, because there are too few peaks and most peaks are broad and overlap. Fig. 2 is a TEM image showing that the sample contains many tubular structures with little dispersion in their diameters. The tubular nature of the material was confirmed as follows. A single tube was selected first. This tube was then tilted along its tube axis and its diameter was monitored while the sample was tilted. The diameter was found to remain constant for different tilting angles (over 32°) about its axis, confirming the tubular nature of the nanostructures. The diameters of the tubes were found to be about 9 nm, with an inner diameter of around 5 nm. The lengths of the tubes ranged from several tens to several hundreds of nanometers. The peaks in the XRD profile were broadened because of the nanometer size of the tube and the bending of some atom planes of the tube.

HRTEM experiments were performed to reveal the atomic structures of the nanotubes. Fig. 3(*a*) is a typical HRTEM image showing a single nanotube. The Fourier transformation of the image area outlined in Fig. 3(*a*) is shown in Fig. 3(*b*). All diffraction spots are elongated in the direction perpendicular to the tube axis. It can be seen from Fig. 3(*a*) that the tube is a very well crystallized multi-wall nanotube with an inter-shell spacing of around 0.78 nm. Compared to the well known carbon nanotubes, the tubes shown in Fig. 3(*a*) have the following characteristics:

(i) Most of the nanotubes are not symmetric. The one shown in Fig. 3(*a*) has four shells on the upper side (with each dark line corresponding to one shell of the tube) but five shells on the lower side. This indicates that the nanotube is scroll type, and this is also evidenced by Fig. 3(*c*), which shows a cross-sectional view of a single nanotube. When electrons are incident perpendicular to the tube axis, a multi-walled scroll tube will sometimes be imaged asymmetrically showing one more shell on one side of the tube than the other side depending on the relative direction of the tube with respect to the incident electron beam.

(ii) Almost all the nanotubes are observed to have open ends, while in many cases carbon nanotubes have caps associated with their ends.

(iii) All nanotubes observed are multi-walled nanotubes. The inter-shell spacing of the multi-walled nanotubes is 0.78 nm, which is much larger than that of the carbon nanotubes (0.34 nm), and the structures of different shells are well correlated.

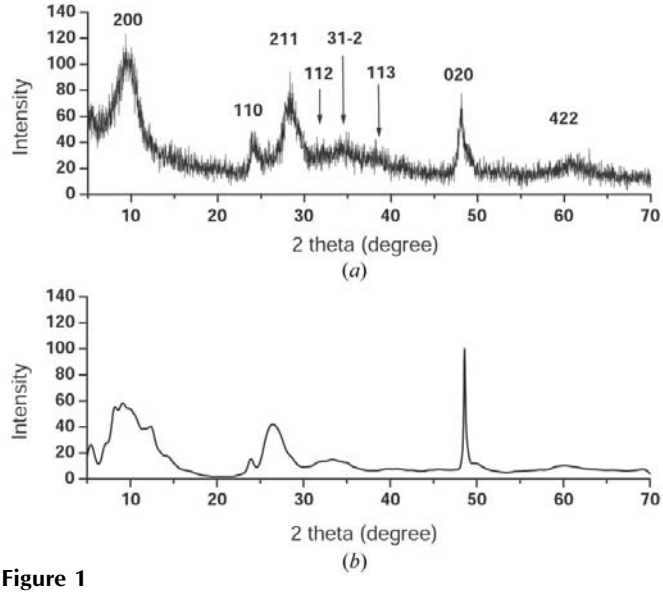

Figure 1
(*a*) Experimental XRD profile taken from nanotubes and (*b*) simulated XRD profile using the trititanate nanotube model.

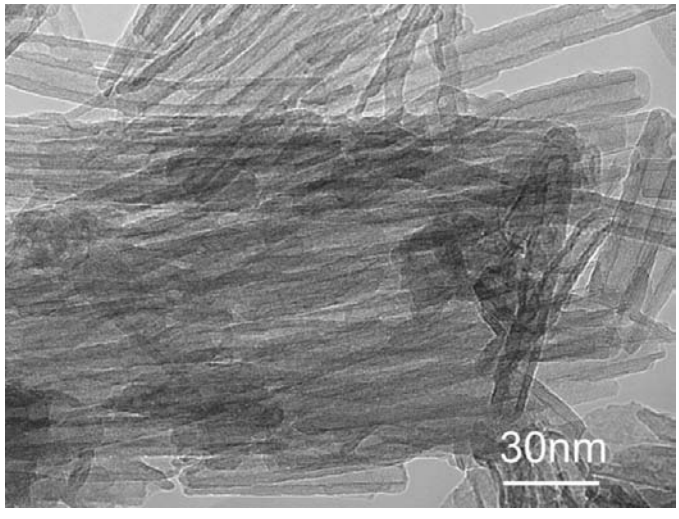

Figure 2
A low-magnification TEM image showing nanotubes about 9 nm in diameter lying preferentially along the horizontal direction.

3.2. The composition of the nanotube

Energy-dispersive X-ray spectroscopy (EDX) and EELS were used to analyze the composition of the nanotube. The former is suitable for detecting heavy elements while the latter is more sensitive to light ones. The EDX study was performed on individual nanotubes using nanoprobe mode on the FEG TEM and a 200 keV accelerating voltage. Only the free-standing isolated nanotubes were selected in experiments to avoid effects due to the supporting carbon film and other nanotubes.

EELS on a single tube was performed using the entrance aperture in the GIF system as the selected-area aperture. The size of the aperture in the objective plane was decided by the magnification of the image. Fig. 4(*a*) shows part of a nanotube being selected by the entrance aperture for EELS analysis. In this case, the section of the tube contributing to the EELS is about 40 nm long. The corresponding EELS spectrum is shown in Fig. 4(*b*); only Ti and O were found by EELS analysis. The counts in the Ti edge and the O edge were calculated after background subtraction. The same background windows and peak windows were used for different spectra. The ratio between the Ti counts and O counts calculated from spectra taken from four different tubes varied by about 20%.

Chemical analysis showed that our sample contained about 2%wt hydrogen, suggesting the possible existence of H in the nanotube. To determine whether the hydrogen signal comes from water absorption on the surface of the sample or from the nanotubes, an IR spectroscopy test was performed. The sample was heated at 403 K for several hours to get rid of adsorption water just before the test. The IR spectrum obtained (shown in Fig. 5) shows a stretching vibration of O—

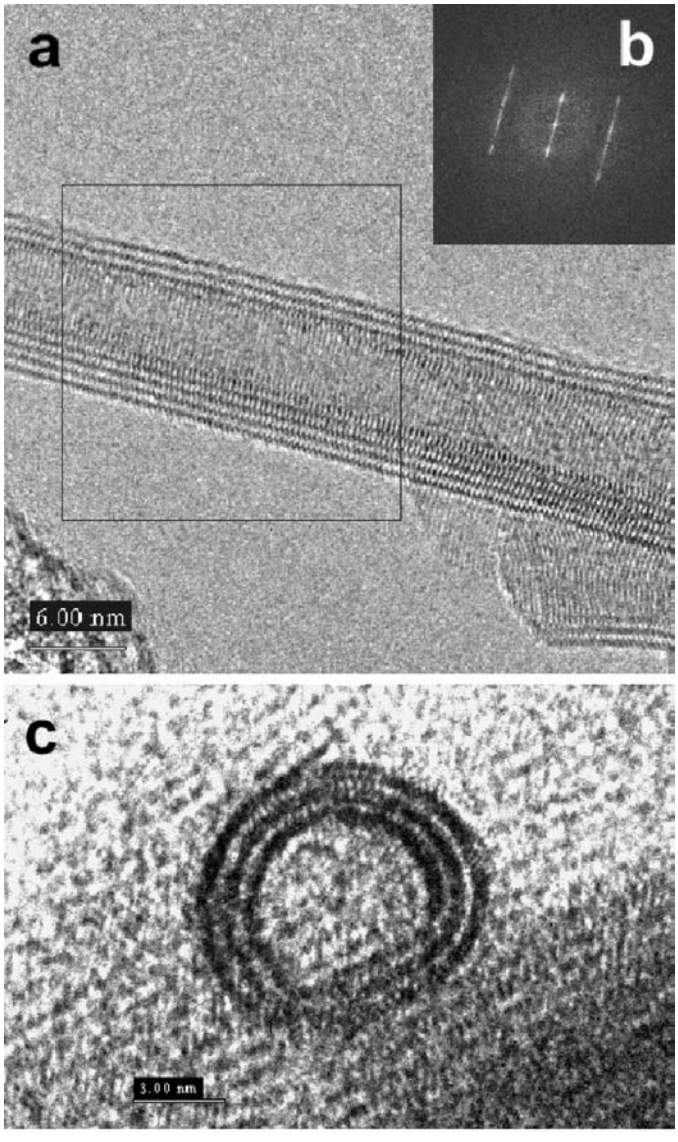

Figure 3
(*a*) An HRTEM image showing a single multi-walled nanotube with an inter-shell spacing of about 0.78 nm. (*b*) Fourier transformation of the selected area of (*a*). (*c*) A cross-sectional view of a single nanotube showing the scroll nature of the nanotube.

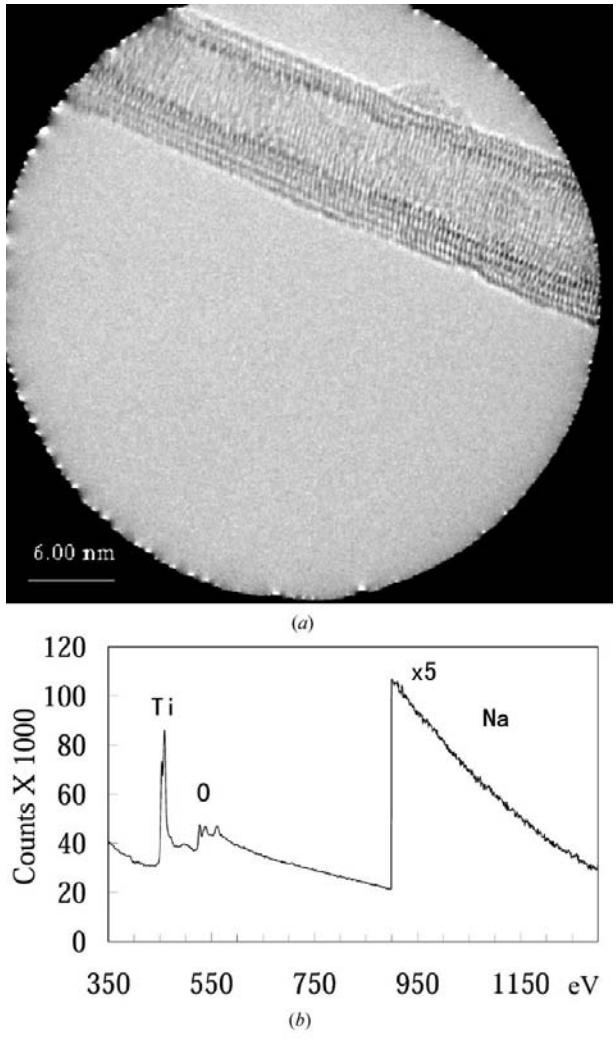

Figure 4
(*a*) An HRTEM image showing a single nanotube being selected by the entrance aperture of the GIF for EELS analysis. (*b*) EELS spectrum obtained from the single nanotube shown in (*a*); only Ti and O peaks are observed.

H around 3400 cm^{-1} and a bending vibration of H—O—H around 1630 cm^{-1}, indicating that bonded H exists within the nanotubes. We conclude that the nanotube is composed of Ti, O and H.

3.3. The structure of the nanotube

For samples that are too small to be studied by X-ray diffraction, electron crystallography provides the best tool for structure determination. The most widely used methods of electron crystallography are basically trial-and-error methods involving structural model building, image and diffraction simulations, and comparison with experimental results. Although these types of methods are not very efficient and often depend on the investigator's prior knowledge of the materials, they remain the most popular ones and, indeed, the most reliable ones, because simulations may take into account the dynamic nature of high-energy electron diffraction. In recent years, progress has been made on the so-called '*ab initio*' methods (Dorset, 1995), which use either electron diffraction data or combined HREM and diffraction data together with a method for the determination of the reflection phases (*e.g.* direct methods). However, the validity of the '*ab initio*' methods is not well established for the general case, because direct methods do not account for any dynamical effects in the electron diffraction data. Theoretically, the use of the '*ab initio*' methods has been justified for some special cases, for example, for small angles of scattering (Peng & Wang, 1994) and for thin crystals composed of identical atoms (Peng, 2000). Experimental justification has been obtained for a wide range of materials by the excellent agreement between the recovered structures and the experimental data (*e.g.* Weirich *et al.*, 1996, 2000; Downing *et al.*, 1990; Dorset, 1995, 1996, 1998). In principle, nanostructured materials provide an ideal subject for the '*ab initio*' methods of electron crystallography, since these materials are small by definition and dynamical effects are not as important as in larger crystals. For our nanotubular materials, however, X-ray crystallographic methods failed to determine the structure from diffraction profiles such as the one shown in Fig. 1(*a*). We do not expect electron diffraction crystallography to do any better in this particular case, since, in general, the quality of electron diffraction data will not be much better than that of X-ray data and few usable diffraction data exist [see Figs. 6 and 7(*b*) for diffraction patterns from polycrystalline and single crystalline samples]. Therefore, we decided to use the conventional real-space trial-and-error approach, *i.e.* we derived the structure model based on all the information we could obtain from the sample and verified the model by comparing the simulated X-ray and electron microscopy data with the experimental results.

Fig. 6 shows a selected area electron diffraction (SAED) pattern taken from an area that is about 1 μm in diameter and contains many nanotubes. Diffraction rings are observed since the sample is polycrystalline with nanotubes oriented along all directions. It should be noted, however, that the intensity distribution along the rings is not uniform. This is because the tubes are not oriented randomly but aligned preferentially along some directions. Fig. 2 shows clearly that all nanotubes in the figure are preferentially aligned horizontally. The innermost ring of Fig. 6 corresponds to a *d*-spacing of 0.78 nm, which agrees with HRTEM observations [see Figs. 2(*a*) and 9]. We note, however, that this *d*-spacing does not show up in the corresponding XRD profile (Fig. 1*a*). The discrepancy between the SAED pattern and the XRD profile occurs mainly because the strength of the electron–specimen interaction is many times stronger than that of XRD. The 0.78 nm period corresponds to the inter-shell spacing of the multi-walled nanotubes perpendicular to their tube axis. Since most

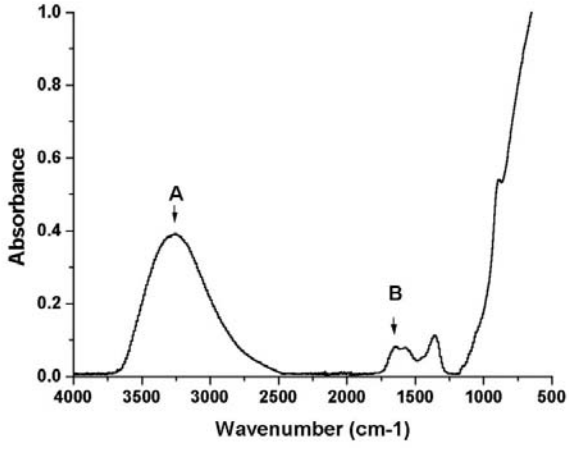

Figure 5
IR spectrum taken from nanotube samples showing a stretching vibration of O—H around 3400 cm^{-1} (A) and a bending vibration of H—O—H around 1630 cm^{-1} (B), indicating the existence of bonded H in the nanotube samples.

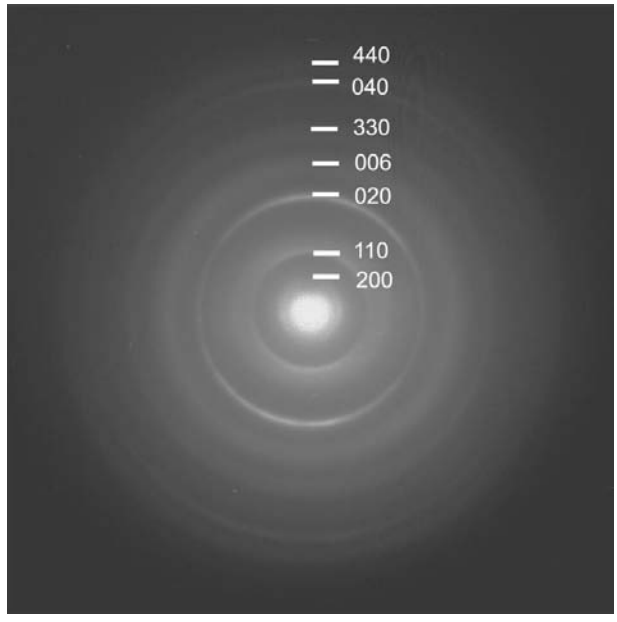

Figure 6
An SAED pattern taken from an area containing a large number of nanotubes. The pattern is indexed using the $H_2Ti_3O_7$ structure.

of the nanotubes have only two to four shells, this periodicity is short ranged. Although two to four shells is sufficient to generate observable features in the electron diffraction pattern, it is not enough to generate appreciable peaks in the XRD profile. A diffraction pattern from a single nanotube has also been obtained. Fig. 7(*a*) shows the image of two nanotubes positioned at an angle of 83° to each other. Fig. 7(*b*) shows the corresponding SAED pattern taken from these two single nanotubes. Only a few spots are observed. The electron diffraction spots are seen to be elongated along the direction perpendicular to the tube axis as the atomic planes are curved in the wrapping direction. The experimental electron diffraction from a single nanotube is similar to the Fourier transformation of experimental HRTEM images such as the one shown in Fig. 3(*b*).

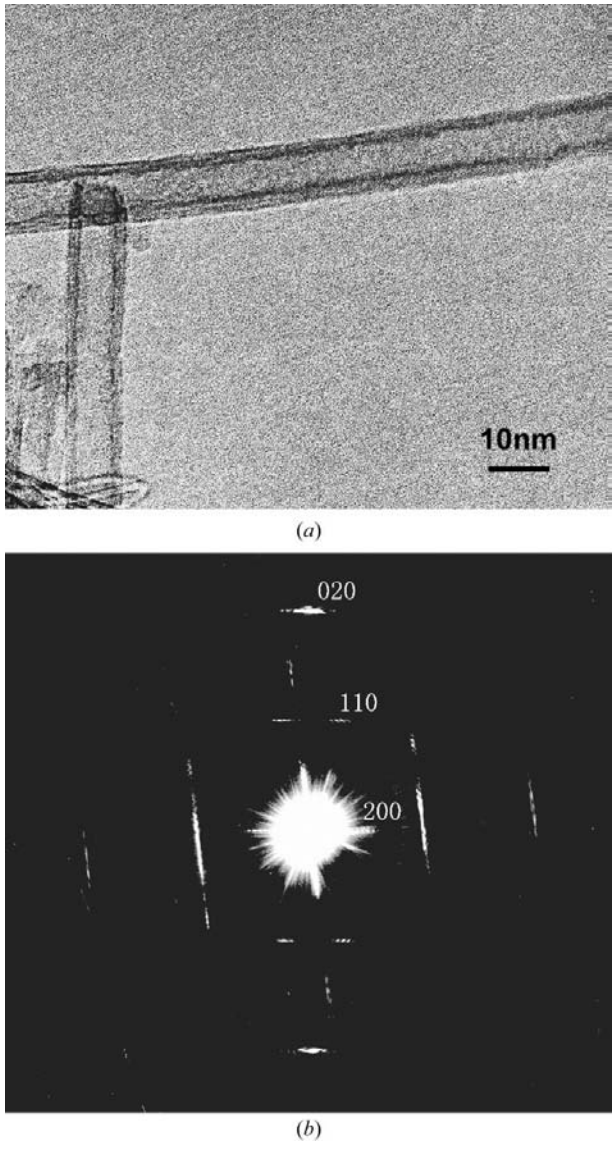

Figure 7
(*a*) TEM image showing two nanotubes at an angle of 83° and (*b*) corresponding SAED pattern. Electron diffraction spots in (*b*) resulting from the horizontal nanotube are indexed using the $H_2Ti_3O_7$ structure.

Table 1
XRD data and SAED data from trititanate nanotubes (*d*-values) in comparison with XRD data of $H_2Ti_3O_7$.

The unit cell of $H_2Ti_3O_7$ is monoclinic with $a = 16.03$, $b = 3.75$, $c = 9.19$ Å and $\beta = 101.45°$

XRD	SAED	$H_2Ti_3O_7$	h	k	l	2θ ($\lambda = 0.154$ nm) for $H_2Ti_3O_7$
9.26	–	9.01	0	0	1	9.54
–	7.80	7.86	2	0	0	11.2
3.67	3.68	3.65	1	1	0	24.4
3.15	3.10	3.08	2	1	1	29.0
2.76	–	2.77	1	1	2	32.3
2.66	2.63	2.67	3	1	−2	33.5
2.36	2.36	2.37	1	1	3	37.9
1.89	1.88	1.88	0	2	0	48.4
1.52	1.54	1.54	4	2	2	60.0
–	1.50	1.50	0	0	6	61.8
–	1.22	1.22	3	3	0	78.3
–	0.94	0.94	0	4	0	110.0
–	0.91	0.91	4	4	0	115.6

From EELS, EDX and IR experiments, we have gained a fair idea about the composition of the nanotubes. We now consider the derivation of an atomic model for our nanotubes. From XRD and electron diffraction experiments, we know that the nanotubes are crystalline. Plane distances can be obtained from powder XRD and SAED from a large area. HRTEM and single-crystal electron diffraction give not only plane distances but also the angles between the planes. Combining the information obtained from XRD, electron diffraction and HRTEM, we obtain nine independent plane distances. After searching through all H—Ti—O compounds with known crystal-plane spacings and angles between these planes, we found that only $H_2Ti_3O_7$ (monoclinic, $a = 16.03$, $b = 3.75$, $c = 9.19$ Å and $\beta = 101.45°$) (Feist & Davies, 1992) fits our experimental data well (see Table 1). Fig. 8(*a*) shows a structural model of 2×2 unit cells of the $H_2Ti_3O_7$ crystal looking along the [010] direction. The structure of $H_2Ti_3O_7$ is seen to be composed of corrugated ribbons of edge-sharing TiO_6 octahedrons. The ribbons are three octahedrons wide, and these octahedrons join at the corners to form a 'stepped' layered structure. The interlayer spacing of the $H_2Ti_3O_7$ crystal is 0.78 nm, which is the same as that observed in the nanotubes using SAED and HREM. In $H_2Ti_3O_7$, H atoms are located between the layers, but these atoms are not shown in Fig. 8(*a*) for clarity. The SAED pattern shown in Fig. 6 is indexed using the $H_2Ti_3O_7$ structure.

To study the crystal orientation of the nanotubes, SAED patterns taken from single nanotubes were indexed. In Fig. 7(*b*), diffraction spots from the vertical nanotube of Fig. 7(*a*) are indexed based on the $H_2Ti_3O_7$ structure. From electron diffraction patterns like Fig. 7(*b*), we determined that the tube axis is parallel to [010] and the electron beam is incident at the central region of the tube (the top and bottom sheets of the tube, which are perpendicular to the incident beam) along [001].

We now proceed to propose an atomic model for the nanotube. The model is based on the layered structure of

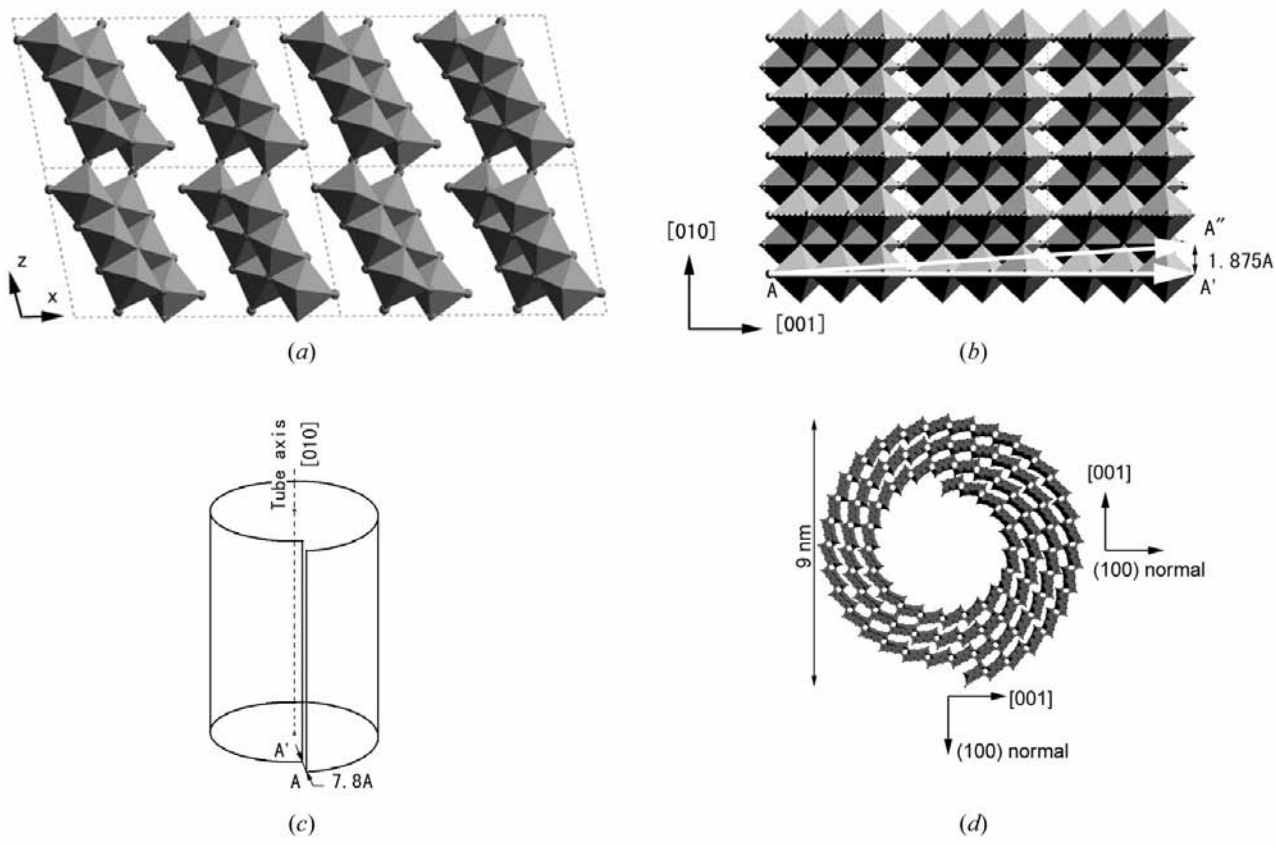

Figure 8
Structure models of (*a*) 2 × 2 unit cells of $H_2Ti_3O_7$ on the [010] projection and (*b*) a layer of $H_2Ti_3O_7$ on the (100) plane from which the nanotube is constructed. AA′ and AA″ indicate the chiral vectors. Schematic diagrams show (*c*) the introduction of a displacement vector AA′ when wrapping up a sheet to form a scroll-type nanotube and (*d*) the structure of the trititanate nanotube. The crystal orientations indicated are the orientations according to the $H_2Ti_3O_7$ layer.

$H_2Ti_3O_7$. The structure of a layer of TiO_6 octahedrons is shown in Fig. 8(*b*), together with the coordinate system used for indexing the structure. For the simplest tube structure, the tube axis is along [010], and the tube may be constructed by wrapping a (100) plane of the atoms shown in Fig. 8(*b*) along the line AA′. While a perfect nanotube, such as a carbon nanotube, may be formed by joining points A and A′, a scroll nanotube may be constructed by displacing the point A′ outward by a layer spacing of 0.78 nm, as shown in Fig. 8(*c*). Fig. 8(*d*) shows a cross-sectional view of a multi-walled scroll nanotube formed by four layers of atoms, and this model is used for simulating the HRTEM image shown in Fig. 9. Viewing along [001] (from the bottom of the figure to the top), the model shows clearly that incident high-energy electrons will 'see' four layers of atoms on the right-hand side of the nanotube but only three layers of atoms on the left-hand side of the nanotube. Consequently, the projected potential and therefore the HRTEM image of the tube will be asymmetric as shown in Fig. 9. A helical angle may also be introduced such that point A is joined to point A″ instead of point A′ (see Fig. 8*b*).

Using the atomic model shown in Fig. 8(*d*), XRD and HRTEM image simulations were performed using *CERIUS*[2] software, and these were compared with experimental results. In the XRD simulation, powder X-ray diffraction was selected and the source used was again Cu $K\alpha$. The tube length was chosen to be 50 nm. Fig. 1(*b*) shows a simulated XRD profile that matched the experimental one shown in Fig. 1(*a*) reasonably well. HRTEM image simulations were made using the model shown in Fig. 8(*d*). The parameters used in the simulation were Cs = 1.2 mm, defocus = −54.86 nm, defocus spread = 7.5 nm, beam spread = 0.5 mrad, vibration = 0.35 nm and aperture size = 0.7 nm^{-1}. Fig. 9 shows an enlarged section of the experimental HRTEM image shown in Fig. 3(*a*), in which two simulated images are inserted (marked in the figure by arrows). During simulations, we found that the experimental image details in the upper-left and bottom-right parts of Fig. 9 could not be matched simultaneously simply by changing simulation parameters (such as defocus values *etc.*). Different tube models with different helical angles had to be introduced to fit the experimental image. The simulated image inserted to the left of the figure is calculated using a model with a helical angle, while the simulated image inserted to the right of the figure is calculated using a model without helicity, as shown in Fig. 8(*b*). The excellent agreement achieved between the simulated and the experimental images indicates that the main features of our model are correct. The fact that we have to use different tube models with different helical

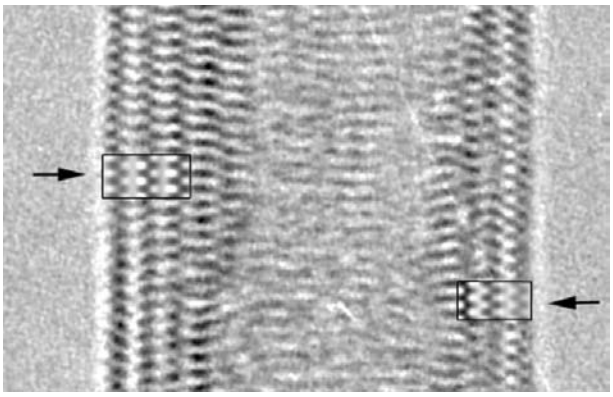

Figure 9
An enlarged section of the experimental HRTEM image shown in Fig. 3(*a*). The inserts are two simulated images of the trititanate nanotube (outlined). The simulated image inserted to the left of the figure is calculated using a model nanotube with a helical angle, while the simulated image inserted to the right of the figure is calculated using a model nanotube without helicity.

angles to fit the experimental image suggests that the tube may contain defects causing helicity changes within a single nanotube. We note that the agreement between the simulated XRD profile and the experimental XRD profile shown in Fig. 1(*a*) is not as good as that achieved in Fig. 9 for HREM images. The discrepancy may result from several factors, including the facts that the sample is not a 100% pure nanotubular sample and that many defects exist in the nanotube; we cannot generally separate diffraction effects due to these defects from those due to nanotubes as easily as we have done in real-space imaging.

4. Conclusion

We have successfully synthesized nanoscale tubular materials *via* the reaction of TiO_2 and NaOH aqueous solution, and the products are shown to be composed of Ti, O and H using EDX, EELS and IR. The tubular structure of the H—Ti—O compound is investigated using the combined techniques of XRD, SAED, HREM and image simulations, and a trititanate nanotube model is derived that is shown to be able to explain all our experimental results. This trititanate nanotube model is based on the layer structure of crystalline $H_2Ti_3O_7$ with a monoclinic unit cell ($C2/m$, $a = 16.03$, $b = 3.75$, $c = 9.19$ Å, $\beta = 101.45^\circ$). Either closed or scroll nanotubes may be constructed, and helicity may be readily introduced in the model. HRTEM observations reveal that the synthesized nanotubes are typically scroll-type multi-walls nanotubes, with an inter-shell spacing of 0.78 nm. An ideal nanotube with zero helical angle may be constructed by wrapping a (100) sheet of $H_2Ti_3O_7$ along the [001] direction with the tube axis parallel to the [010] direction.

This work was supported by the Ministry of Science and Technology of China (Grant No. 001CB610502) and Peking University. We would like to thank Dr W. Z. Zhou and Professor X. F. Duan for useful discussions.

References

Accelrys (2002). http://www.accelrys.com/cerius2/.
Adachi, M., Murata, Y. & Harada, M. (2000). *Chem. Lett.* **8**, 942–943.
Chopra, N. G., Luyken, R. J., Cherry, K. & Crespi, V. H. (1995). *Science*, **269**, 966–967.
Dagan, G. & Tomkiewicz, M. (1993). *J. Phys. Chem.* **97**, 12651–12655.
Dorset, D. L. (1995). *Structural Electron Crystallography*. New York: Plenum Press.
Dorset, D. L. (1996). *Acta Cryst.* B**52**, 753–769.
Dorset, D. L. (1998). *Acta Cryst.* A**54**, 750–767.
Downing, K. H., Meisheng, H., Wenk, H. & O'Keefe, M. A. (1990). *Nature* (*London*), **348**, 525–528.
Du, G. H., Chen, Q. & Peng, L.-M. (2001). *Appl. Phys. Lett.* **79**, 3702–3704.
Feist, T. P. & Davies, P. K. (1992). *J. Solid State Chem.* **101**, 275–295.
Feldman, Y., Wasserman, E. & Srolovitz, D. A. (1995). *Science*, **267**, 222–225.
Fukishima, A. & Honda, K. (1972). *Nature* (*London*), **238**, 37.
Fukushima, K. & Yamada, I. (1989). *J. Appl. Phys.* **65**, 619–623.
Hsu, W. K., Zhu, Y. Q., Boothroyd, C. B., Kinloch, I., Trasobares, S., Terrones, H., Grobert, N., Terrones, M., Escudero, R., Chen, G. Z., Colliex, C., Windle, A. H., Fray, D. J., Kroto, H. W. & Walton, D. R. M. (2000). *Chem. Mater.* **12**, 3541–3546.
Iijima, S. (1991). *Nature* (*London*), **354**, 56–58.
Kasuga, T., Hiramatsu, M. & Hoson, A. (1998). *Langmuir*, **14**, 3160–3163.
Kasuga, T., Hiramatsu, M., Hoson, A., Sekino, T. & Niihara, K. (1999). *Adv. Mater.* **11**, 1307–1311.
Niederberger, M., Muhr, H. J., Krumeich, F., Bieri, F., Gunther, D. & Nesper, R. (2000). *Chem. Mater.* **12**, 1995–2000.
Peng, L.-M. (2000). *Acta Cryst.* A**56**, 511–518.
Peng, L.-M. & Wang, S. (1994). *Acta Cryst.* A**50**, 759–771.
Tenne, R., Margulis, L. & Genut, M. (1992). *Nature* (*London*), **360**, 444–446.
Weirich, T., Ramlau, R., Simon, A., Hovmoller, S. & Zou, X. D. (1996). *Nature* (*London*), **382**, 144–146.
Weirich, T. E., Zou, X. D., Ramlau, R., Simon, A., Cascarano, G. L., Giacovazzo, C. & Hovmöller, S. (2000). *Acta Cryst.* A**56**, 29–35.
Weng-Sieh, Z., Cherrey, K., Chopra, N. G. & Blase, X. (1995). *Phys. Rev. B*, **51**, 11229–11232.